Search for Neutrinoless Double Beta Decay in Xenon 136 with the Enriched Xenon Observatory (EXO)

P.C. Rowson[*][†]

SLAC

E-mail: rowson@slac.stanford.edu

The EXO collaboration has during its first year of running reached its performance goals for background control and energy resolution, and is producing scientific results. The collaboration has previously reported the first observation of two-neutrino double-beta decay [1], a result that resolved a puzzling mismatch between theory and a published limit [2]. Here we report on a search for neutrinoless double-beta decay of ^{136}Xe with EXO-200 [3]. No signal is observed for a ^{136}Xe exposure of 26.3 kg-yr, with a background of $\sim 1.5 \times 10^{-3}$ kg(^{enr}LXe)$^{-1}$yr^{-1}keV^{-1} in the $\pm 1\sigma$ region of interest. This sets a lower limit on the half-life of the neutrinoless double-beta decay $T_{1/2}^{0\nu\beta\beta}$(^{136}Xe) $> 1.6 \times 10^{25}$ yr (90% CL), corresponding to effective Majorana masses of less than 140–380 meV, depending on the matrix element calculation. This result significantly constrains published reports of the observation of the neutrinoless mode in ^{76}Ge [4].

36th International Conference on High Energy Physics
4-11 July 2012
Melbourne, Australia

---

[*]Speaker.

[†]Representing the EXO Collaboration

1. Introduction

The $0\nu\beta\beta$ decay rate is related to the square of an effective Majorana neutrino mass $\langle m \rangle_{\beta\beta}$ by the product of a phase space factor and a nuclear matrix element squared. Kinematic measurements restrict the neutrino mass scale to be below $\mathcal{O}(1\text{ eV})$ [5], leading to $0\nu\beta\beta$ half lives beyond 10^{24} yr. A search for $0\nu\beta\beta$ decay in ^{76}Ge has claimed a positive observation [4] with $T_{1/2}^{0\nu\beta\beta}(^{76}\text{Ge})= (2.23^{+0.44}_{-0.31}) \times 10^{25}$ yr, implying $\langle m \rangle_{\beta\beta} = 0.32 \pm 0.03$ eV for the nuclear matrix element given in [6]. The $2\nu\beta\beta$ decay has been observed in many isotopes [7] and, recently, in ^{136}Xe with the EXO-200 detector [1], later confirmed in [8]. A high resolution measurement of the decay electron sum energy allows discrimination between the two decay modes.

EXO-200, described in detail in [9], uses xenon both as source and detector for the two electrons emitted in its $\beta\beta$ decay. The detector is a cylindrical homogeneous time projection chamber (TPC) [10]. It is filled with liquefied xenon (^{enr}LXe) enriched to $(80.6\pm0.1)\%$ in the isotope ^{136}Xe. The remaining 19.4% is ^{134}Xe, with other isotopes present only at low concentration. EXO-200 is designed to minimize radioactive backgrounds, maximize the ^{enr}LXe fiducial volume, and provide good energy resolution at the ^{136}Xe Q-value of 2457.83 ± 0.37 keV [11]. Energy depositions in the TPC produce both ionization and scintillation signals. The TPC configuration allows for three-dimensional topological and temporal reconstruction of individual energy depositions. This ability is essential for discriminating $\beta\beta$ decays from residual backgrounds dominated by γs.

The cylindrical TPC (Figure 1) is divided into two symmetric volumes separated by a cathode grid. Each end of the TPC is instrumented with 38 charge induction (V) and 38 charge collection (U) wire triplets. Each triplet provides a single charge readout with a pitch of 9 mm. The U and V wire grids, crossing at $60°$, provide stereoscopic information on the topology of the charge deposition. At each end of the TPC there are $\sim$250 Large Area Avalanche Photodiodes (LAAPDs) [12], read out in groups of mostly 7, that record the 178 nm scintillation light. A drift field of 376 V/cm is applied in the TPC volume. All signals are digitized at 1 MS/s in frames of ± 1024 samples around every physics trigger (produced by either charge collection or scintillation signals). All detector components were carefully selected to minimize internal radioactivity [13]. The TPC is mounted in the center of a low-background cryostat. At least 50 cm of high purity HFE-7000 fluid [14] and at least 25 cm of lead shield the TPC from external radioactivity. The ^{enr}LXe is continuously purified in gas phase by recirculation [15] through hot Zr getters [16], with electron lifetimes of $\sim$3 ms achieved. A calibration system allows the insertion of radioactive sources to various positions immediately outside of the TPC. The clean room module housing the TPC is surrounded on four sides by an array of 50 mm thick plastic scintillator panels, serving as a cosmic ray veto. Cosmic ray muons traversing the TPC are detected at $(95.5 \pm0.6)\%$ efficiency. EXO-200 is located at a depth of (1585^{+11}_{-6}) m.w.e. at the Waste Isolation Pilot Plant (WIPP), near Carlsbad, New Mexico, USA.

EXO-200 started taking low background data in late May 2011. Data collected until August 2011 was used to measure the $2\nu\beta\beta$-decay rate of ^{136}Xe [1]. In preparation for taking the data covered in this paper, some detector upgrades were performed, improving the performance of the electronics and of the lead shielding. The data presented here was collected from September 22, 2011 to April 15, 2012, for a total of 2,896.6 hours live time under low background conditions. During the same period, 376.8 hours of calibration data were collected with three γ sources at three
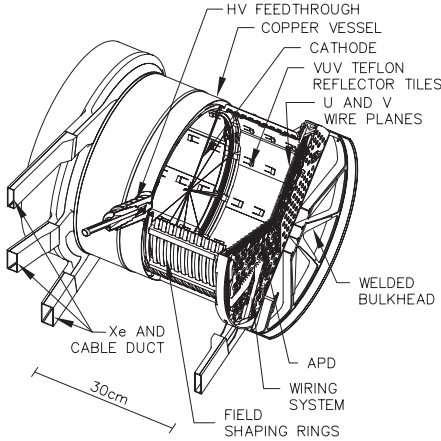
Figure 1: The cylindrical EXO-200 TPC. A central cathode divides the device into two separate drift regions, with each (anode) end intrumented for scintillation light and stereoscopic charge readout.
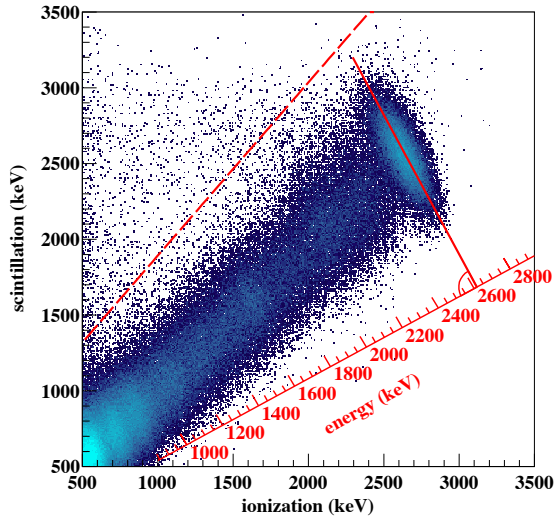

Figure 2: Correlation between ionization and scintillation for SS events from a ^{228}Th source. Events in the top-left quadrant are due to incomplete charge collection and are rejected by the cut (dashed line), removing only 0.5% of the total. The cut is defined using the gamma ray full absorption islands from three calibration sources.

positions. Most of this data was taken with a ^{228}Th source for the primary purpose of measuring the free electron lifetime (τ_e) in the TPC.

Offline event reconstruction proceeds in three stages: signal finding, parameter estimation, and clustering. Charge signals on the U wires and scintillation signals on the two LAAPD planes are found using a matched filter technique. The filter yields time estimates for both ionization and scintillation channels. The time information from the U wires is used to search for induction signals in V wire waveforms. A signal un-shaping algorithm is applied to the U wire waveforms, optimizing the discrimination between single-site (SS) and multiple-site (MS) energy depositions. Candidate U wire signals are fit to template waveforms modeling the measured transfer functions so that the signal amplitudes can be extracted for energy estimation. Amplitudes are corrected, channel-by-channel, for electronic gains determined from radioactive source calibration. U wire and V wire signals are then combined into charge clusters using timing information from the fits, and associated with the nearest (earlier in time) summed scintillation signal. Each cluster energy is corrected for position-dependent charge losses due to finite ^{enr}LXe purity and for the shielding grid inefficiency of the V wire plane. This procedure yields a reconstructed ionization energy and three dimensional position information for each charge cluster. An efficiency loss is incurred by events for which 3D reconstruction is not possible as these are rejected from this analysis.

Figure 2 shows the energy of events as measured by the ionization and scintillation channels while the ^{228}Th source was deployed. As first discussed in [17] and evident from the tilt of the 2615 keV full absorption ellipse in the figure, the magnitude of the two signals is anticorrelated.

The 2D SS and MS energy spectra are independently rotated and projected onto a new (1D) energy variable in such a way as to minimize the width of the 2615 keV γ line. It is found that $\sigma/E = 1.67\%$ (1.84%) for SS (MS) spectra at $Q_{\beta\beta}$, dominated by the noise and broadening terms.

The ability of the TPC to identify SS and MS interactions is used to separate β and $\beta\beta$ decays in the bulk xenon from multiple site γ interactions. The clustering, currently applied in 2D, has a separation resolution of 18 mm in the U-dimension and 6 mm in z (drift time). The SS and MS spectra are compared to probability density functions (PDFs) generated by GEANT4 [18] and detector simulations (MC). This procedure reproduces the shape of the ^{60}Co and ^{228}Th source spectra. The MC reproduces the fraction of SS events, defined as $N_{SS}/(N_{SS} + N_{MS})$, to $\pm 8.5\%$. In addition, for ^{228}Th ($0\nu\beta\beta$) events the simulation predicts a 70% (71%) efficiency for the requirement that events are fully reconstructed in 3D. The simulation predicts the absolute, NIST-traceable, activity of all sources to within $\pm 9.4\%$.

The fiducial volume used in this analysis contains 79.4 kg of ^{136}Xe (3.52×10^{26} atoms), corresponding to 98.5 kg of active ^{enr}LXe. The trigger is fully efficient above 700 keV. The cut represented by the dashed diagonal line in Figure 2 eliminates a population of events due to interactions in the ^{enr}LXe region for which the charge collection efficiency is low, leading to an anomalous light-to-charge ratio. This cut also eliminates α decays from the low background data, but causes only a negligible loss of efficiency for γ- and β-like events. Cosmic-ray induced backgrounds are removed using three time-based cuts. Events preceded by a veto hit within 25 ms are removed (0.58% dead time). Events occurring within 60 s after a muon track in the TPC are also eliminated (5.0% dead time). Finally, any two events that occur within 1 s of each other are removed (3.3% dead time). The combination of all three cuts incurs a total dead time of 8.6%. The last cut, combined with the requirement that only one scintillation event per 2 ms of read out waveform is observed, removes β-α decay coincidences due to the time correlated decay of the ^{222}Rn daughters ^{214}Bi and ^{214}Po. Alpha spectroscopic analysis finds $360 \pm 65\ \mu$Bq of ^{222}Rn in the ^{enr}LXe, constant in time.

The SS and MS low background spectra are shown in Figure 3. Primarily due to bremsstrahlung, a fraction of $\beta\beta$ events are MS. The MC predicts that 82.5% of $0\nu\beta\beta$ events are SS. Using a maximum likelihood estimator, the SS and MS spectra are simultaneously fit with PDFs of the $2\nu\beta\beta$ and $0\nu\beta\beta$ of ^{136}Xe along with PDFs of various backgrounds. Background models were developed for various components of the detector. Results of the material screen campaign, conducted during construction, provide the normalization for the models. The contributions of the various background components to the $0\nu\beta\beta$ and $2\nu\beta\beta$ signal regions were estimated using a previous generation of the detector simulation [9].

The $2\nu\beta\beta$ PDF is produced using the Fermi function calculation given in [19]. Tests using a slightly different spectral form [20] were performed and found to contribute $<0.001\%$ to the predicted location of $Q_{\beta\beta}$.

For the best-fit energy scale and resolution the $\pm 1\sigma$ and $\pm 2\sigma$ regions around $Q_{\beta\beta}$ are shown in Figure 4. The number of events observed in the SS spectrum are 1 and 5, respectively, with the 5 events in the $\pm 2\sigma$ region accumulating at both edges of the interval. Therefore, no evidence for $0\nu\beta\beta$ decay is found in the present data set. The upper limit on $T_{1/2}^{0\nu\beta\beta}$ is obtained by the profile likelihood fit to the entire SS and MS spectra. Systematic uncertainties are incorporated as constrained nuisance parameters. The fit yields an estimate of 4.1 ± 0.3 background counts in the
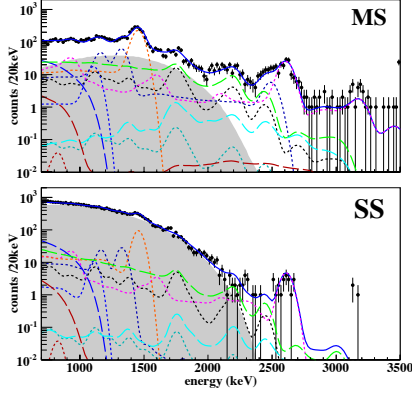
Figure 3: MS (top) and SS (bottom) energy spectra from the 2,896.6 hours of low background data used for this analysis. The best fit line (solid blue) is shown. The background components are $2\nu\beta\beta$ (grey region), ^{40}K (dotted orange), ^{60}Co (dotted dark blue), ^{222}Rn in the cryostat-lead air-gap (long-dashed green), ^{238}U in the TPC vessel (dotted black), ^{232}Th in the TPC vessel (dotted magenta), ^{214}Bi on the cathode (long-dashed cyan), ^{222}Rn outside of the field cage (dotted dark cyan), ^{222}Rn in active xenon (long-dashed brown), ^{135}Xe (long-dashed blue) and ^{54}Mn (dotted brown). The last bin on the right includes overflows. There are no overflows in the SS spectrum.
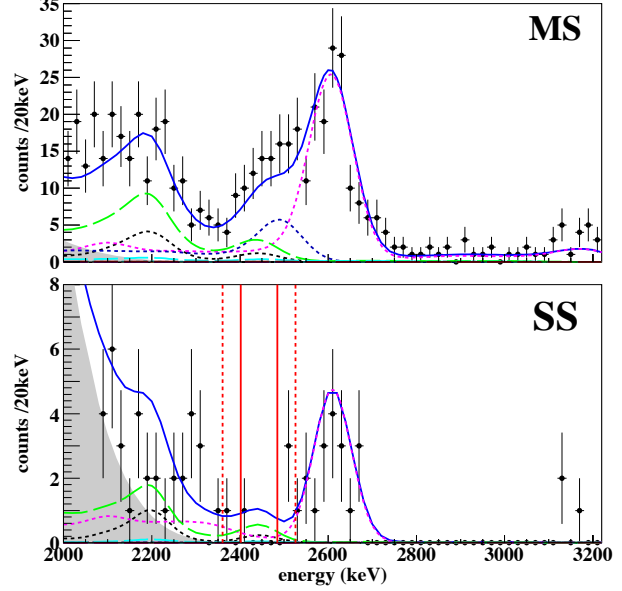

Figure 4: Energy spectra in the ^{136}Xe $Q_{\beta\beta}$ region for MS (top) and SS (bottom) events. The 1 (2)σ regions around $Q_{\beta\beta}$ are shown by solid (dashed) vertical lines. The $0\nu\beta\beta$ PDF from the fit is not visible. The fit results have the same meaning as in Figure 3.

$\pm 1\sigma$ region, giving an expected background rate of $(1.5 \pm 0.1) \times 10^{-3}\,\text{kg}^{-1}\text{yr}^{-1}\text{keV}^{-1}$. The fit also reports $0\nu\beta\beta$ decay limits of < 2.8 counts at 90% CL (< 1.1 at 68% CL). This corresponds to a $T_{1/2}^{0\nu\beta\beta} > 1.6 \times 10^{25}$ yr at 90% CL ($T_{1/2}^{0\nu\beta\beta} > 4.6 \times 10^{25}$ yr at 68% CL). Toy MC studies confirm the coverage of this method as suggested by [21]. The same fit also reports $T_{1/2}^{2\nu\beta\beta} = (2.23 \pm 0.017$ stat. ± 0.22 sys.$) \times 10^{21}$ yr, in agreement with [1] and [8]. The levels of contamination from γ-emitting nuclides are found to be consistent with material screening estimates [13]. The addition to the fit of a PDF for ^{137}Xe produces a 13% higher limit on $T_{1/2}^{0\nu\beta\beta}$ at 90% CL. In the absence of an independent constraint on this cosmogenic background, the smaller limit is reported.

The result from the likelihood fit is compared with the recent constraint for ^{136}Xe [8] and the best limit [22] and claimed detection [4] for ^{76}Ge. The present result contradicts [4] at 68% CL (90% CL) for all (most) matrix element calculations considered [23, 24, 25, 26, 6] and provides upper bounds to Majorana neutrino masses between 140 and 380 meV at 90% CL.

(Note : Recently, the KamLAND Zen Collaboration has released a preprint with updated results that are consistent with all results reported here [27] and which further constrain the validity

of the reported observation of neutrinoless double beta decay.)

Acknowledgments

References

[1] N. Ackerman *et al.* Phys. Rev. Lett. 107 (2011) 212501.

[2] R. Bernabei *et al.* Phys. Lett. B 546 (2002) 23.

[3] M. Auger *et al.* Phys. Rev. Lett. 109 (2012) 032505.

[4] H.V. Klapdor-Kleingrothaus and I.V. Krivosheina, Mod. Phys. Lett., A21 (2006) 1547.

[5] V.N. Aseev *et al.*, Phys. Rev. D 84 (2011) 112003; Ch. Kraus *et al.*, Eur. Phys. J. C40 (2005) 447.

[6] A. Staudt, K. Muto and H. V. Klapdor-Kleingrothaus, Europhys. Lett. 13 (1990) 31.

[7] K. Nakamura *et al.* (Particle Data Group) J. Phys. G 37 (2010) 075021.

[8] A. Gando *et al.* Phys. Rev. C 85 (2012) 045504.

[9] M. Auger *et al.* JINST 7 (2012) P05010.

[10] H. Drumm *et al.* Nucl. Instr. Meth. A 176 (1980) 333.

[11] M. Redshaw *et al.* Phys. Rev. Lett. 98 (2007) 053003.

[12] R. Neilson *et al.* Nucl. Instr. Meth. A 608 (2009) 68.

[13] D.S. Leonard *et al.* Nucl. Instr. Meth. A 591 (2008) 490.

[14] 3M, see http://www.3m.com/product/index.html.

[15] F. LePort *et al.* Rev. Sci. Inst. 82 (2011) 105114.

[16] SAES "MonoTorr", see http://www.saespuregas.com/.

[17] E. Conti *et al.* Phys. Rev. B 68 (2003) 054201.

[18] S. Agostinelli *et al.* Nucl. Inst. Meth. A 506 (2003) 250.

[19] G.K. Schenter and P. Vogel, Nucl. Sci. Eng., 83 (1983) 393.

[20] J. Kotila and F. Iachello, Phys. Rev. C 85 (2012) 034316.

[21] W.A. Rolke, A.M. Lopez and J. Conrad, Nucl. Inst. Meth. A 551 (2005) 493.

[22] H.V. Klapdor-Kleingrothaus *et al.* Eur. Phys. J. A12 (2001) 147.

[23] T.R. Rodriguez and G. Martinez-Pinedo, Phys. Rev. Lett. 105 (2010) 252503.

[24] J. Menendez *et al.*, Nucl. Phys. A 818 (2009) 139.

[25] J. Barea and F. Iachello, Phys. Rev. C79 (2009) 044301 and private communication.

[26] F. Simkovic *et al.*, Phys. Rev. C 79 (2009) 055501.

[27] A. Gando *et al.* arXiv:1211.3863.